LIFETIME ATTRIBUTABLE BREAST CANCER RISK ASSOCIATED WITH RADIATION EXPOSURE FROM CHEST COMPUTED TOMOGRAPHY IN FEMALE COVID-19 PATIENTS IN GEORGIA

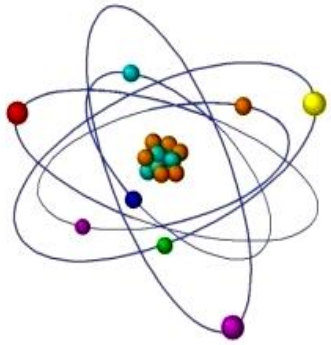

[1,2,3]Tamar Sanikidze, [4]Levan Ratiani, [5,2,3]Giorgi Gavashelishvili, [1]Alla. Zedginidze, [1,2,3]Sophio Kalmaxelidze, [4]Nino. Ormotsadze, [2]Maka. Korkelia, [1,2,3]Giorgi Ormotsadze*

[1] Iv.Beritashvili Center of Experimental Biomedicine, Georgia
[2] Tbilisi State Medical University Georgia
[3] Georgian Association of Medical Physics and Radiaton Protection, Georgia
[4] The First University clinic of Tbilisi State Medical University, Georgia
[5] Radiation Medicine Center, Georgia

https://doi.org/10.63465/rrs520258977 *Correspondingauthor: g.ormotsadze@lifescience.org.ge

ABSTRACT**:** *The study aimed to assess the lifetime attributable risk of breast cancer associated with chest computed tomography (CT) exposure in female COVID-19 patients in Georgia. Data was obtained from the National Center for Disease Control and Public Health of Georgia (NCDCG), concerning COVID-19 morbidity, hospitalization, and mortality rates for the general population during the period 2020–2021. Additionally, information on the age distribution of breast cancer incidence among the female population in Georgia from 2015 to 2023, as well as demographic data from the National Statistical Office of Georgia for the years 2017 to 2019, was used. Furthermore, data from the First University Clinic in 2020, detailing the age and sex distribution of hospitalized patients and survival-mortality indicators, was also incorporated into the analysis. Population doses were modeled using the Log-Normal distribution with mean 14.16 mGr and median 12.82 mGr for adults and for children 4.58 mGr and 4.47 mGr respectively. Age structure of study population were evaluated using a Bayesian approach. A competing risk methodology was employed to estimate both age-conditional and lifetime baseline risks (LBR) of breast cancer development. These estimates were calculated using the United States National Cancer Institute's DevCan software (version 6.9.0). To determine the age-conditional and lifetime attributable risk (LAR) of radiogenic breast cancer, the methodology outlined in the 2006 report by the Biological Effects of Ionizing Radiation (BEIR) VII Committee of the National Academies of Sciences was applied. Risk computations were performed using the National Cancer Institute's RadRAT software and the LARisk R package. Monte Carlo simulation techniques were used to estimate uncertainties in risk and subjective uncertainties under various assumptions.*

It was shown that the lifetime attributable risk for Breast cancer in female COVID patients in Georgia, related to chest computed tomography in one year is low - 12.77 [90% UR 3.20 - 29.90], and is only 0.2% of the lifetime baseline risk (LBR) for breast cancer. However, for the population under 40 years of age, this ratio is already 2.2%. Overall, the projected number of future breast cancer cases that could be attributed to a chest CT scan performed in one year is 20.06 [90% UR 5.02 - 46.96] cases. Given the cumulative effects of ionizing radiation and the potential risk of multiple or repeated scanning, further improvements in methods for predicting the long-term effects of medical radiation exposure appear necessary.

Keywords: Lifetime attributable breast cancer risk, chest computed tomography

INTRODUCTION

The unique diagnostic efficacy of computed tomography has led to a dramatic increase in the frequency of its use - over the past two decades, the number of CT scans in the United States increased from 57 million to 90 million [1,2]. Accordingly, the dose burdens associated with medical imaging on populations have increased dramatically.

To correctly assess the carcinogenic risks in the range of low doses of radiation and to solve the tasks of regulatory control, the National Research Council of the United States developed a population-specific, age- and sex-dependent methodology for assessing the carcinogenic risks [3], which, with various modifications and for different purposes, is currently widely used by both international and national regulatory organizations [4,5,6]. The World Health Organization used this methodology to assess and predict the medical consequences of the Fukushima incident [7]. Based on this methodology, it was shown in 2007 that approximately 1.5–2% of the total cancer incidence in the United States could be associated with computed tomography [8]. The prognostic values of the cancer risk associated with CT imaging were estimated according to the scanning zones; it has been shown that of the total number of associated with CT scans cancers (78 million scans) performed in the United States in 2007 (n=29,000 (95% UR, 15,000-45,000)), the most contributed were abdomen and pelvis (n = 14,000) (95% UR, 6,900-25,000) and chest (n = 4,100) (95% UR, 1,900-8,100) [9]. In subsequent years, large-scale epidemiological studies conducted in different countries [10-13] quantitatively verified and confirmed theoretical estimates of carcinogenic risks associated with CT. Among them, we would like to highlight a study by British scientists, where 178,604 patients were retrospectively analyzed, and it was revealed that compared with patients who received a dose of less than 5 mGy, the relative risk of leukaemia for patients who received a cumulative dose of at least 30 mGy was 3·18 (95% CI 1·46–6·94) and the relative risk of brain cancer for patients who received a cumulative dose of 50–74 mGy was 2·82 (1·33–6·03) [13].

The carcinogenic risk associated with medical imaging has received particular attention during and after the COVID-19 pandemic, which has been linked to a dramatic increase in chest CT scans in infected patients. For example, a multicenter study of 42,028 chest computed tomography scans found that total radiation exposure increased by 573% in patients screened in 2019, with the highest increase seen in the 20–29 age group (18.6-fold) [14]. Numerous studies, both international and national, have examined the radiation doses to the breast and lungs from chest CT scans using different protocols in populations and their prognostic values for carcinogenic risk in children, adults, and the elderly [15–22]. International expert organizations and regulatory bodies have been developing recommendations for minimizing doses and risks in chest CT by “justifying” and “optimizing” the procedures, taking into account the epidemiological situation, clinical situation, patient category, etc. [23-28].

In Georgia, prognostic assessments of the increase in oncological morbidity associated with the Covid-pandemic are not found in the literature available to us, while the aforementioned information seems to us to be very relevant, both in terms of identifying priority areas of the National Cancer Control Strategy in Georgia, In Georgia, prognostic assessments of the increase in oncological morbidity associated with the Covid-pandemic are not found in the literature available to us, while the aforementioned information seems to us to be very relevant, both in terms of identifying priority areas of the National Cancer Control Strategy in Georgia, as well as in terms of further refining the theoretical foundations of “justification” – “optimization” in computed tomography and regulatory control. In our earlier studies, radiogenic carcinogenic risk projection models for breast and lung sites were developed for the Georgian population based on the BEIR VII methodology [29]. This paper will present and discuss prognostic estimates of the increase in cancer incidence associated with the COVID-19 pandemic in the Georgian female population.

MATERIALS AND METHODS

Data was obtained from the National Center for Disease Control and Public Health of Georgia (NCDCG), concerning COVID-19 morbidity, hospitalization, and mortality rates for the general population during the period 2020–2021. Additionally, information on the age distribution of breast cancer incidence among the female population in Georgia from 2015 to 2023, as well as demographic data from the National Statistical Office of Georgia for the years 2017 to 2019, was used. Furthermore, data from the First University Clinic in 2020, detailing the age and sex distribution of hospitalized patients and survival-mortality indicators, was also incorporated into the analysis.

Organ (Breast) radiation dose in chest CT was evaluated from imaging protocols using the software CT-Expo V 2.8. Population doses were modeled using the Log-Normal distribution with mean 14.16 mGr and median 12.82 mGr for adults and for children 4.58 mGr and 4.47 mGr respectively. Age structure of study population were evaluated using a Bayesian approach. A competing risk methodology was employed to estimate both age-conditional and lifetime baseline risks (LBR) of breast cancer development. These estimates were calculated using the United States National Cancer Institute's DevCan software (version 6.9.0). To determine the age-conditional and lifetime attributable risk (LAR) of radiogenic breast cancer, the methodology outlined in the 2006 report by the Biological Effects of Ionizing Radiation (BEIR) VII Committee of the National Academies of Sciences was applied [3,4]. Risk computations were performed using the National Cancer Institute's RadRAT software and the LARisk R package. Monte Carlo simulation techniques were used to estimate uncertainties in risk and subjective uncertainties under various assumptions [30,31,32].

RESULTS

Before proceeding directly to the discussion of the results, we consider it appropriate to emphasize a few important points for further discussion clarification. The modern standard of quantitative hazard characteristics (quantitative risk characterization) imposes qualitatively new requirements on its content and accuracy. "Health risk assessment" is considered as a "process that includes determining (estimating) the health risk associated with the harmful effects of an external factors including the identification of attendant uncertainties [33]. The concept of "uncertainties" is fundamentally different from the classical "errors", namely, when measuring any quantity, it is necessary to indicate the conditions and circumstances under which the measurement is carried out, the full realization of which is in principle impossible, since it requires infinitely large amounts of information. Therefore, there always remains an area of subjective interpretation (informational uncertainty). This component may be, or may not be, of minimal importance, but its indication is considered necessary [32], especially when objects of high potential danger are characterized [34,35]. The modern standard considers the "uncertainty" of measurement (evaluation) as the sum of two types of uncertainty (Type A and Type B). Type A uncertainty - a random statistical error, for the evaluation of which standard statistical procedures are used, Type B uncertainty - does not decrease with an increase in the number of repeated measurements, and is evaluated by scientific judgment based on all of the available information on the possible variability of the measurand (in particular, the results obtained in earlier studies, expert assessments, etc.).

The main stages of uncertainty assessment according to Joint Committee for Guides in Metrology [30,31,32] are a) formulation (defining the input and output quantities, developing a model relating input and output quantities, on the basis of available knowledge assign probability density function (PDF) to each individual input), b) propagation (propagating PDF input data through the model to produce PDF output data) and c) summary.

Formulation:

First, it should be noted that, since the present study belongs to uncontrolled and unstructured observational studies, only B-type uncertainty is considered. As mentioned above, the study aimed to estimate the The population-averaged lifetime attributable risk (LAR) of Breast Cancer $((LAR)\bar{}\_P\hat{}Breast)$ and the age structure of the increase in cancer incidence ($N\_D\hat{}P\ (e)$) in the population infected with COVID-19 in Georgia irradiated in 2021 (Output quantities).

Our analysis of these characteristics is based on the BEIR VII methodology modified by the US EPA [3,4]. In the BEIR VII approach, the lifetime attributable risk (LAR) for each cancer site is the main measure of risk. It represents the lifetime probability of developing cancer in a hypothetical (100,000 people) exposed cohort and depends on 1) the demographic age-sex structure, 2) the age-sex structure of mortality, and 3) the age-sex structure of the background cancer incidence rate. Accordingly, it is specific for each population, including the Georgian population.

In the case of breast cancer, it has the following form:

$$\begin{aligned}&\langle\!\langle \boldsymbol{LAR} \rangle\!\rangle\ \hat{}\boldsymbol{Breast}\ (\boldsymbol{D},\boldsymbol{e})\\&\quad=\boldsymbol{D}*\boldsymbol{\beta}\int\_(\boldsymbol{e}+\boldsymbol{L})\hat{}\boldsymbol{100}\ \langle\!\langle \boldsymbol{exp}\,[(\boldsymbol{\gamma}(\boldsymbol{e}-\boldsymbol{25}))/\boldsymbol{10}]\ (\boldsymbol{a}/\boldsymbol{50})\hat{}\boldsymbol{\eta}*(\boldsymbol{S}(\boldsymbol{a}))\\&\quad/\ (\boldsymbol{S}(\boldsymbol{e}))*\boldsymbol{da}\ \ (\boldsymbol{1})\rangle\!\rangle\end{aligned}$$

Where D is the radiation dose, e is the age at exposure, a is the attained age, and β is the coefficient, which reflects the radiosensitivity of the study population (in this approach, the difference in radiosensitivity between populations is ignored). S(a) is the probability of surviving to age a, and L is the minimum latency period of developing cancer.

The following parameter values are recommended by the US EPA for breast cancer: β = 10; γ = -0.50; η= 3.5 for a < 50 and 1,1 for a > 50. These values are universal for all populations, the difference is only in the mortality curve S(a). From equation (1), by simple transformations, we can obtain $(LAR)\bar{}\_P\hat{}Breast$ and $N\_D\hat{}P\ (e)$:

$$\begin{aligned}&(\boldsymbol{LAR})\bar{}\boldsymbol{\_P\hat{}Breast}\\&\quad=\boldsymbol{D}\\&\quad/(\boldsymbol{N\_D\hat{}P}\ )\int\_\boldsymbol{0\hat{}100}\ \langle\!\langle \boldsymbol{N\_D\hat{}P}\ (\boldsymbol{e})\ \ \langle\!\langle \boldsymbol{LAR} \rangle\!\rangle\ \hat{}\boldsymbol{Breast}\ (\boldsymbol{D},\boldsymbol{e})\boldsymbol{de}\rangle\!\rangle\ \ (\boldsymbol{2})\end{aligned}$$

$$\boldsymbol{N\_P\hat{}Breast}\ (\boldsymbol{e},\boldsymbol{D})=\boldsymbol{D}\int_{\boldsymbol{e}}^{\boldsymbol{100}}\boldsymbol{N\_D\hat{}P}(\boldsymbol{e})[(\ \langle\!\langle \boldsymbol{LAR} \rangle\!\rangle\ \hat{}\boldsymbol{Breast}\ (\boldsymbol{D},\boldsymbol{e}))/\boldsymbol{100000}]\boldsymbol{de}\quad(\boldsymbol{3})$$

In this equations $N\_D\hat{}P\ (e)$ - the age structure of the irradiated in 2021 COVID-19 patients, and $N\_D\hat{}P=\int\_0\hat{}100\ \langle\!\langle N\_D\hat{}P\ (e)de\rangle\!\rangle$ - is their total number.

Equation (3) represent the models that relating the output quantities ($(LAR)\bar{}_P\hat{}Breast$and $N\_P\hat{}Breast\ (e,D)$), with input quantities, which in our case are considered: 1) $\langle\!\langle LAR \rangle\!\rangle\ \hat{}Breast\ (D,e)$ - lifetime attributable risk of developing breast cancer in a population irradiated with a dose D on the age of e, 2) $N\_D\hat{}P\ (e)$ - the age structure of the irradiated population and 3) D - the radiation dose, the value of which depends on a number of factors (the model of the CT scanner, the protocols used, the qualifications of the radiologists, the clinical status of the patient, etc.), these quantities are random variables, so the next stage of the study was the assessment of their probability density functions (PDF).

We described the PDF of the lifetime risk of developing breast cancer for each age group by a normal (Gaussian) distribution:

$$\langle\!\langle \boldsymbol{LAR} \rangle\!\rangle\ \hat{}\boldsymbol{Breast}\ (\boldsymbol{D}=\boldsymbol{10mGr},\boldsymbol{e}=\boldsymbol{e\_i})=\mathbf{N}\left(\boldsymbol{\mu}_{\boldsymbol{e_i}},\boldsymbol{\sigma}_{\boldsymbol{e_i}}\right)\ \ (\boldsymbol{4})$$

The mean values ($\boldsymbol{\mu_{e_i}}$) and standard deviation ($\boldsymbol{\sigma_{e_i}}$), for each $\boldsymbol{e_i}$age group were taken from our earlier work [29], where the age-dependent lifetime attributable risk of Breast Cancer (number of cancer cases per 100,000 persons) for the Georgian female population irradiated with a dose D = 10 mGy was estimated (Figure 1).

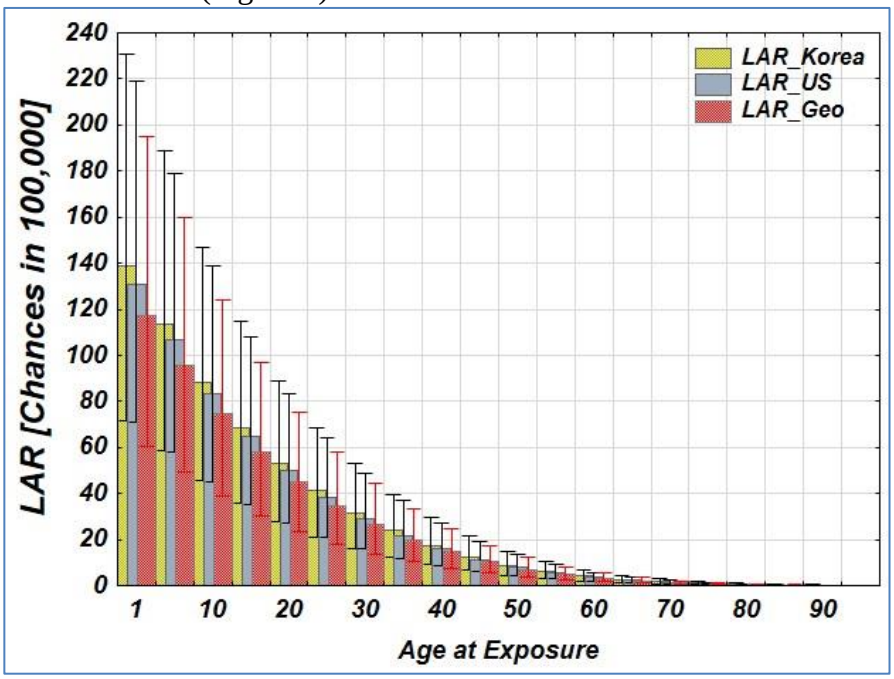

Figure 1. Distributions of lifetime attributable risk for female populations of Georgia, the United States, and Korea irradiated at a dose of 10 mGy. Whiskers – 95% uncertainty range

As for the age structure of the exposed population and the probability distribution functions of radiation doses, at the moment, the quantitative characteristics of the dose loads associated with the COVID-19 pandemic in the population of Georgia, as well as the age structure of the exposed population are not available to us, therefore, the assessment of these distributions seems possible only on the basis of indirect data and analysis of literature data; From this position, we consider it appropriate to first analyze the available information on the criteria for categorizing infected patients, the use of CT imaging in different categories of patients, imaging protocols and dose selection criteria.

The following classifiers proposed by the Fleischner Society provide general ideas about these criteria (criteria for "justifying" the diagnostic procedure) [23].

Severity of respiratory disease (*Mild: no evidence of significant pulmonary dysfunction or damage (eg, absence of hypoxemia, no or mild dyspnea), Moderate to severe: evidence of significant pulmonary dysfunction or damage (eg, hypoxemia, moderate-to-severe dyspnea)*

Pretest probability (*Based on background prevalence of disease as estimated by observed transmission patterns. May be further modified by individual's exposure risk. Subcategorized as: Low: sporadic transmission, Medium: clustered transmission, High: community transmission).*

Risk factors for disease progression (*Present: clinical judgment regarding combination of age .65 years and presence of comorbidities (eg, cardiovascular disease, diabetes, chronic respiratory disease, hypertension, immune-compromised).*

Resource constraints *(Limited access to personnel, personal protective equipment, COVID-19 testing ability (including swabs, reagent, or personnel), hospital beds, and/or ventilators with the need to rapidly triage patients).*

In addition to these criteria in terms of "justification" of the procedure, an important factor is considered the informative value of computed tomography in terms of diagnosing the disease, severity of the course, development of complications and prognosis of lethal outcome. The analysis of a number of clinical studies revealed that CT imaging has low specificity - Imaging findings are nonspecific and share commonalities with other infections such as influenza, H1N1, (SARS-CoV-1) and MERS-CoV [38], along with this, because the risk of infection transmission across imaging personnel and other patients, without known or suspected COVID-19 infections, is high [45], the United States Center for Disease Control and Prevention (CDC) does not recommend using chest radiographs or CT scans as a screening method or first-line diagnostic tool for COVID-19 [24],. Similarly, the American College of Radiology (ACR) advises against using CT scans for screening or diagnosing COVID-19, stating that such imaging should only be performed in specific cases involving hospitalized, symptomatic patients [25]. The Fleischner Society also shared this position. According to these recommendations, CT imaging is recommended only for monitoring complications of COVID-19 in hospitalized patients and for special case indications [23].

Somewhat different principles are observed in the approaches of Chinese specialists [26,27], who believe that although RT-PCR is the gold standard for diagnosis, high false negative results, which delay patient isolation and treatment initiation, increase the risk of persistent transmission of infection and the risk of complications Taking these circumstances into account, Chinese experts recommend the use of CT imaging in unconfirmed cases (screening, diagnosis), in cases of high Pretest probability and probable false negative test results. Pediatric cases require a separate discussion. Children are more vulnerable than adults to the effects of radiation dose, therefore, chest CT in children must only be performed when RT-PCR and immunoassays are not available and/or urgent information is needed in children with severe disease. [23]. As for the practice of using radiological imaging methods in COVID-19 patients in Georgia, it is regulated by the National Guidelines for the Clinical Management of Infection Caused by the Novel Coronavirus (SARS-CoV-2) (COVID-19) in Adult and Pediatric Patients [https://sms.tsmu.edu/ssms/cme/img/ax_co_ga_inf.pdf], according to which chest radiological examination (radiography, computed tomography) is recommended for adult hospitalized patients with both possible and confirmed COVID-19, although the study protocol is not specified. In children with lung damage caused by COVID-19, chest X-ray is considered necessary, and if this study is uninformative, computed tomography is recommended. Based on the above, with a high degree of certainty, the population of hospitalized COVID-19 patients in Georgia can be considered as a irradiated contingent.

The National Center for Disease Control and Public Health of Georgia registered 908,908 infected and 157,047 hospitalized patients of both sexes in 2021, but the literature available to us does not provide information on the age distribution of hospitalized patients by sex. Statistical reports reflect only the age structure of patients discharged from the clinic without gender details (Figure 2), while the age structure of hospitalized patients of different sexes may differ significantly, as indicated by the 2020 data of the First University Clinic of Tbilisi State Medical University on the sex and age structure of hospitalized patients (Figure 3)

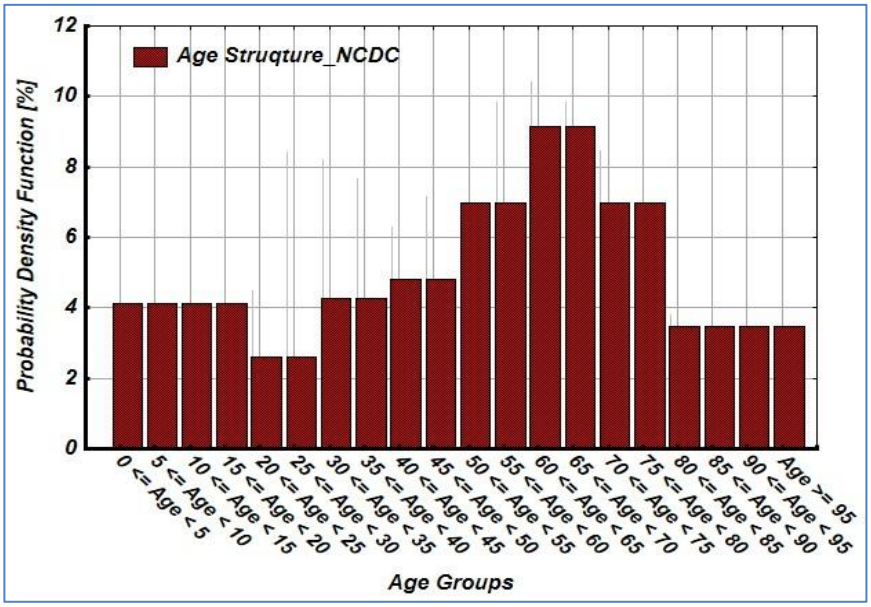

Figure 2. Age structure of patients discharged from clinics in 2021 across Georgia (NCDCG)

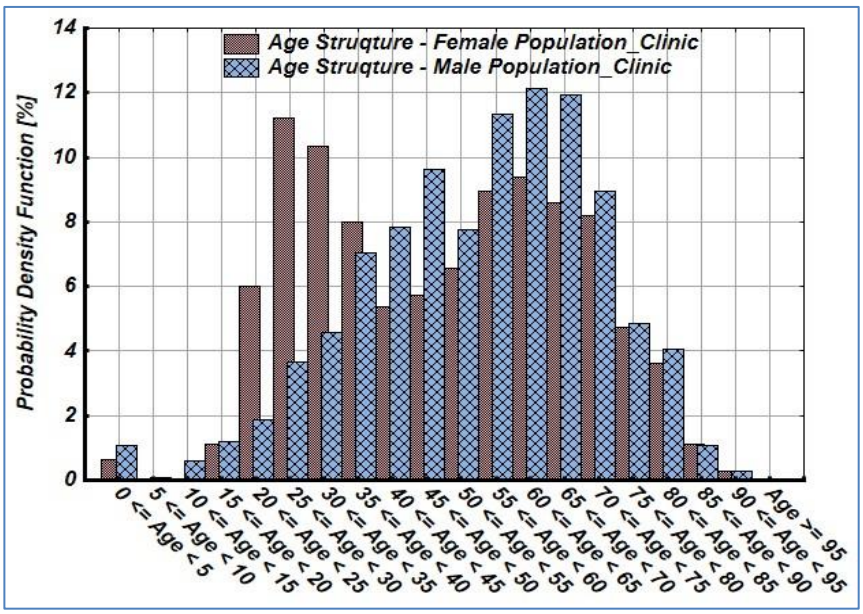

Figure 3. Age and sex structure of patients hospitalized at the First University Clinic of Tbilisi State Medical University in 2020

As can be seen from Figure 2 and Figure 3, the clinic data on the age structure of the female population, which is a bimodal distribution with maxima in the age ranges τ=25-35 and τ=60-70 years, qualitatively differs from the NCDCG data, which is an asymmetric bell-shaped function with a maximum in the age ranges τ=60-70 years. The reason for the identified difference, as we see it, is related to the uncertainties of the clinic and NCDCG data, the first of which is related to sampling error, while in relation to NCDC it should be associated with the insufficient quality of discretization by age and the averaging of data by sex. A literature review on the age structure of hospitalized patients of different sexes (Figure 4) partially coincide with the data of both the clinic and the NCDCG (therefore, they do not have additional information value).

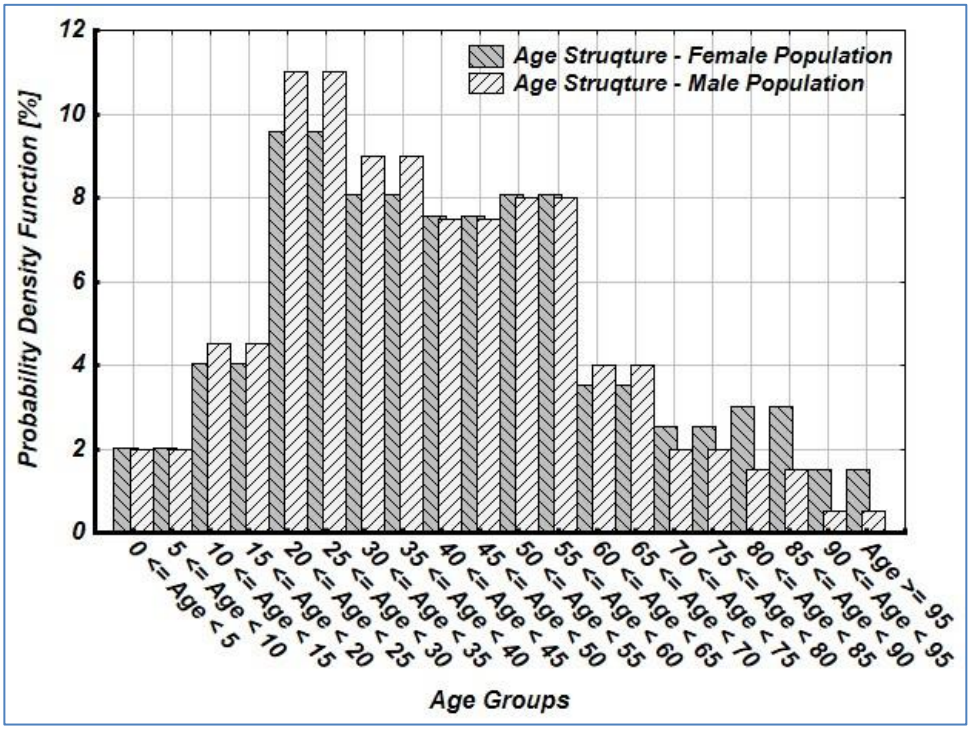

Figure 4. Age and sex structure of COVID-19 infected patients. (German population 2021, patient status unknown) [39]

Given the above stated, for the optimal use of the available information on the age and sex structure of the exposed population, it was considered appropriate to use the Bayesian approach, which allows integrating estimates obtained from various sources, including experiential estimates, which classical, frequency-based probability and statistics cannot provide. The approach is based on Bayes theorem of conditional probability, which is expressed in the following mathematical formula:

$$\boldsymbol{P(A|B) = \frac{P(B|A)\cdot P(A)}{P(B)}} \quad . . \quad .(\mathbf{4})$$

Where:
P(A|B) – the probability of event A occurring, given event B has occurred (posterior)
P(B|A) – the probability of event B occurring, given event A has occurred (likelihood)
P(A) – the probability of event A (prior)
P(B) – the probability of event B
In essence, the above theorem specifies the probability P(A) of the realization of some event (A), if occurring some event (B), independent of it. This makes it possible to integrate information obtained from various sources, including "expert estimation" into the study of a specific problem, which significantly reduces the "uncertainties" associated with the estimates and increases the degree of "reliability" of the results. All these factors add high flexibility and efficiency to the research, which is why the use of this methodology in research is recommended by the U.S. Food and Drug Administration [36,37].

Concerning our problem, quantity A is the probability (p_i) of a patient falling into some $\boldsymbol{\tau_i \div \tau_{i+1}}$ age group. The above-mentioned NCDCG data on the age structure of hospitalized patients (Figure 2) provide some, although incomplete, information on the distribution of $\boldsymbol{p_i}$; therefore, $\boldsymbol{P^{NCDCG}(p_i)}$ can be considered as the a posteriori distribution of $\boldsymbol{p_i}$.
In the case of known p_i, in any random sample of the study cohort, in our case in the cohort of patients hospitalized in the first university clinic ($\boldsymbol{N^{clinic}}$), the probability of a patient falling into the age group

$\boldsymbol{\tau_i \div \tau_{i+1}}$, $P(\boldsymbol{n_f^{clinic}} \mid \boldsymbol{p_i}, \boldsymbol{N^{clinic}})$ can be considered as a "likelihood Function". By integrating these two probabilities in (4), we obtain the age structure of COVID-19-infected and hospitalized female patients in Georgia:

$$\boldsymbol{P(p_i \mid n_f^{clinic}, n_i^{NCDCG}, N^{clinic}, N^{NCDCG}) \propto P(n_f^{clinic} \mid p_i, N^{clinic}) * P^{NCDCG}(p_i)} \quad (5)$$

The distribution of $\boldsymbol{p_i}$ is usually described by a beta-distribution, since the range of definition of this function is [0 1], in our variables it will have the following form:

$$\boldsymbol{P^{NCDCG}(p_i) = \left[\frac{1}{B(n_i^{NCDCG},\ N^{NCDC})}\right] \cdot \left[(p_i)^{(n_i^{NCDCG}-1)} \cdot (1-p_i)^{(N^{NCDCG}-1)}\right]} \ldots (6)$$

Here, $\boldsymbol{N^{NCDCG}}$ - NCDCG data on the total number of COVID-19 hospitalized patients in 2021 (157047 patients), $\boldsymbol{n_i^{NCDCG}}$ - NCDCG data on the age structure of COVID-19 hospitalized patients in 2021 (Figure 2). $\boldsymbol{B(n_i^{NCDC},\ N^{NCDC})}$- is the normalization coefficient in the beta distribution.

In the case of known $\boldsymbol{p_i}$, the number of patients in the age group (likelihood) $\boldsymbol{\tau_i \div \tau_{i+1}}$is described by the binomial statistical distribution:

$$\boldsymbol{P(n_f^{clinic} \mid p_i, N^{clinic}) = \binom{N^{clinic}}{p_i} \cdot p_i^{N^{clinic}} \left(1 - p_i^{N^{clinic}}\right)^{N^{clinic} - n_f^{clinic}}} \ldots (7)$$

By inserting expressions (6) and (7) into expression (5) and further simplifying, we obtain the expression for calculating the posterior distribution:

$$\boldsymbol{P(p_i \mid n_f^{clinic}, n_i^{NCDCG}, N^{clinic}, N^{NCDCG}) \propto p_i^{(n^{clinic} + n^{NCDCG} - 1)} * (1-p_i)^{(N^{clinic} - n_f^{clinic} + N^{NCDCG} - n_i^{NCDCG})}} \quad (8)$$

Using the expression (8), we obtain the distribution functions of patients $\boldsymbol{p_i}$, for a separate $\boldsymbol{\tau_i \div \tau_{i+1}}$ age group of patients (Figure 5), based on which the mean value of the probability, standard deviation, and 95% range of uncertainty were calculated for a separate $\boldsymbol{\tau_i \div \tau_{i+1}}$ age group (Figure 6).

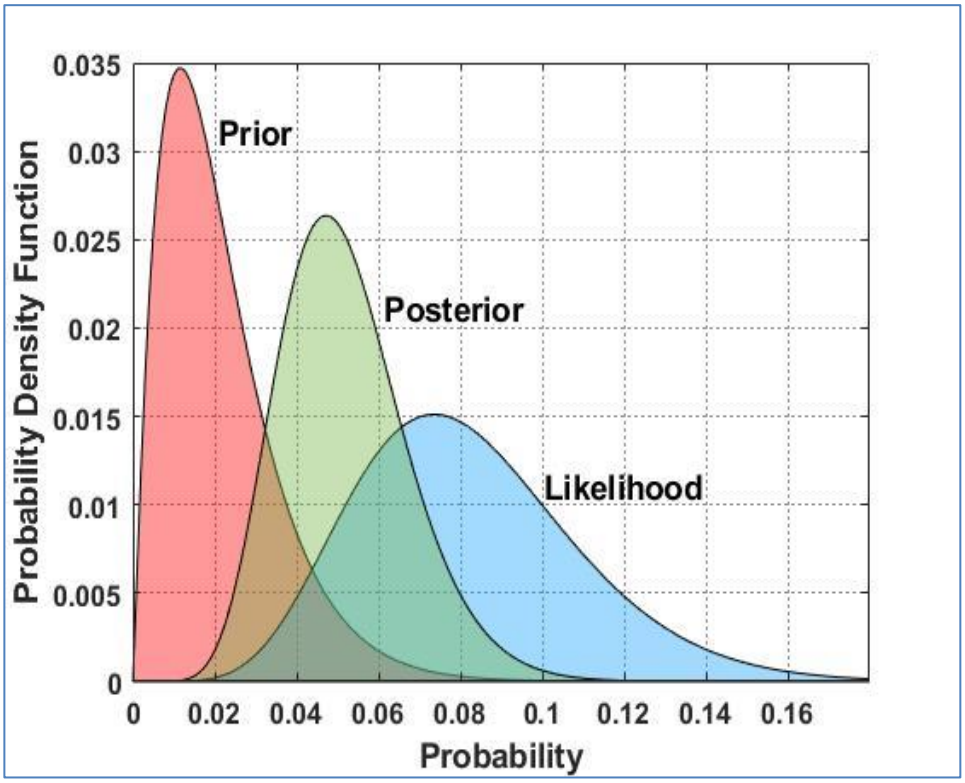

Figure 5. Prior, posteriori, and likelihood distribution functions of hospitalized female COVID-19 patients aged 35-40 years

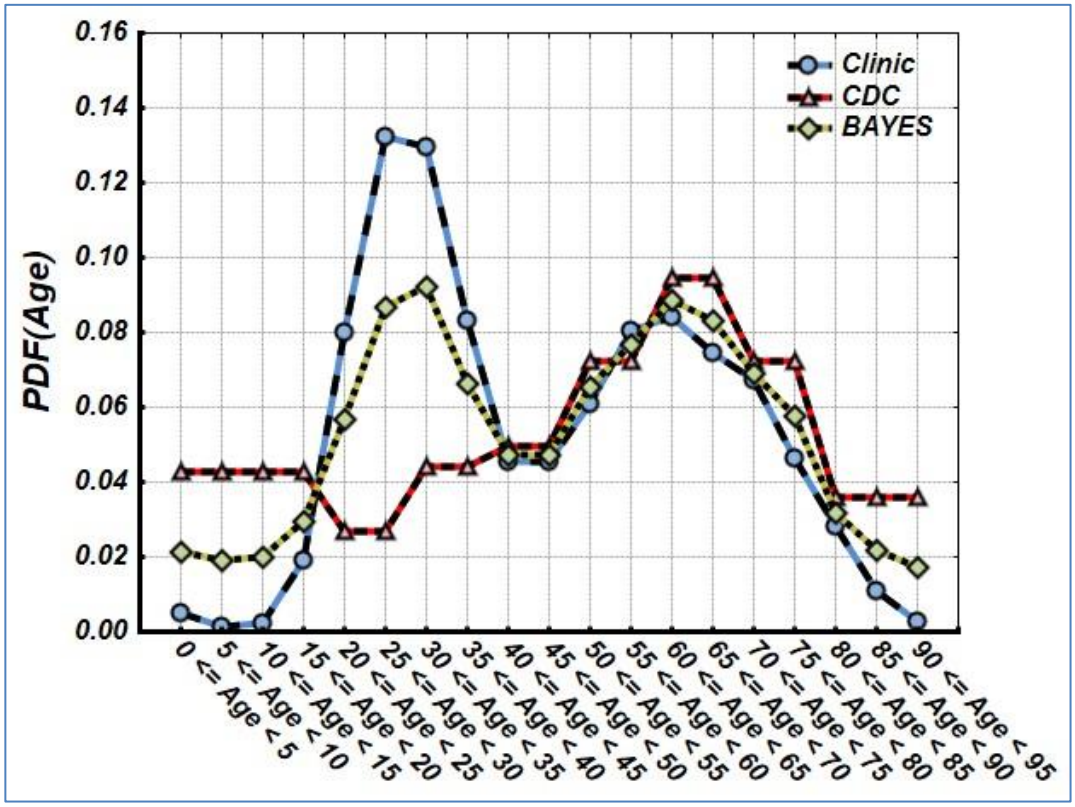

Figure 6. Age distribution of hospitalized women with COVID-19 based on clinic data (circles), NCDCG data (triangles), and estimated using a Bayesian approach (rhombuses)

Scanning techniques (protocols) in COVID-19 patients and doses used

The following general trends emerge regarding recommended CT imaging protocols in COVID-19 patients [23]:

in suspected or known COVID-19 pneumonia report a single-phase, non-contrast chest CT without the need for contrast injection or post-contrast series.

In subjects with suspected pulmonary embolism or necrotizing pneumonia from superimposed bacterial infection, direct post-contrast arterial phase CT can be performed.

There is no evidence to support the use of routine multiphase chest CT in patients with COVID-19 pneumonia.

A webinar [16,17] was organized by the International Atomic Energy Agency (IAEA) to monitor and optimize the dose rates used in medical imaging of COVID-19 patients, with the participation of 62 health care sites from 34 countries on 5 continents. Information on the local prevalence of COVID-19 infection, diagnostic methods, specific protocols and doses was discussed. It was found that than one-half of the health care sites used CT for initial diagnosis of COVID-19 pneumonia and three-fourths used CT for assessing disease severity, approximately 20% of participants used reduced-dose noncontrast chest CT with radiation dose less than the routine or general chest CT

protocol. Approximately 71% of cases used a single examination, 29% used two or more examinations, and approximately 20% used 2 or more phased examinations. There were no significant differences in the doses used between countries, while the doses used at different healthcare providers in the same country varied significantly. There were eightfold variations in median CTDIvol and 10-fold variations in median DLP across multiple participating health care providers from the same country. The medians of the CTDIvol and DLP distributions used varied between 7–11 mGy and 280–439 mGy *cm (absorbed dose of the breast 11.2 – 17.6 mGr*), with a pronounced right-skewed asymmetry (mean/median ≈ 1.106). (Organ (Breast) dose in chest CT was evaluated from imaging protocols using the software CT-Expo V 2.8)

Detailed information on the dose burden associated with CT imaging in COVID patients is presented in a systematic review article [18], which analyzed the results of 81 studies in different countries (China 66.3%, Italy 7.0%; France -4.7%, Iran-3.5%, the United States2.3%). It was found that 23% of CT examinations were used for screening purposes, Regarding the number of CT scans, 14858 patients, 267 patients, and 447 patients had one, two, and three or more CT examinations, respectively. The regimens used varied widely (CTDIvol range 2.3 – 12.6 mGr, (absorbed dose of the breast 4 – 20.8 mGr*), it should be noted that, as presented above, there is no significant difference in the protocols and doses used between different countries. Similar results are observed in other, numerous, international, or national studies [19]. Considering the high dose burden on the population during the COVID pandemic, especially young and pediatric patients, several healthcare providers have developed low-dose chest CT protocols for COVID-19 subjects. Some studies reported an 88–91% reduction in effective dose without compromising the diagnostic image information (CTDIvol 1÷3.5 mGr, DLP 20.4 ÷ 112, kVp 80÷100, mA 10÷50, Pitch 1÷1.7, absorbed dose of the breast 1.6 – 5.6 mGy*), [17, 22]. The most common technical parameters manipulated in low-dose protocols were tube potential and most importantly, tube current (mA).

In Georgia, when modeling the dose burden associated with chest CT in COVID-19 patients, we primarily proceeded from the fact established by the International Atomic Energy Agency that chest CT dose burdens in COVID-infected patients do not differ significantly across countries, while There were eightfold variations in median CTDIvol and 10-fold variations in median DLP across multiple participating health care providers**.** Accordingly, in the absence of a complete data of chest CT dose burdens in Georgia, it was considered more reliable to extrapolate the dose burdens adopted in international practice to the Georgian population**.** Based on the above, we used the asymmetric log-normal distribution to model the Breast absorbed dose during chest CT imaging in COVID-infected patients in Georgia:

$$\boldsymbol{P^{Breast}(D) = Lognormal(\mu, \delta^2)}$$

For the mean value of the normal distribution (μ) associated with the log-normal distribution, a dose of 14.8 mGy was considered optimal, and the value of δ was estimated taking into account the condition Mean (D_{Breast}) /Median (D_{Breast})=1.1 (Figure 7). This approach allows us to assume with a high degree of confidence that the proposed model correctly reflects the central tendencies in the Breast absorbed dose distributions, while the asymmetry of the distribution qualitatively characterizes the share of low-dose protocols and two or more multiple and phased gamma scans in the total dose loads. Similarly, were selected dose parameters for pediatric scanning.

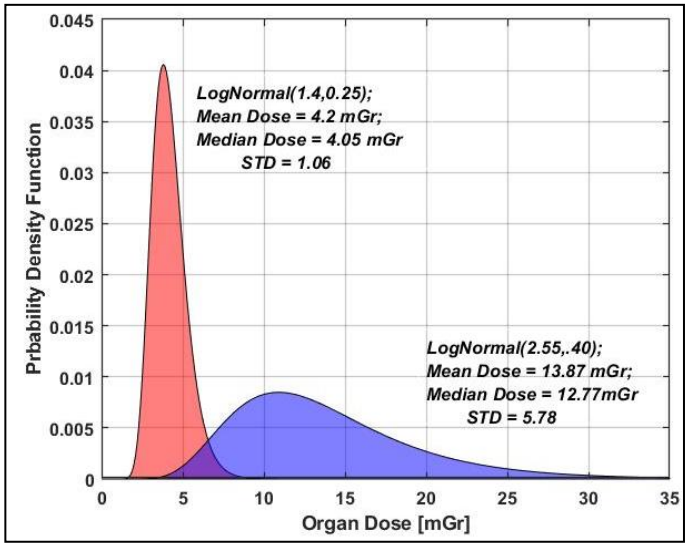

Figure 7. Breast absorbed dose distributions associated with chest CT in the COVID-19 pediatric and adult female patients in Georgia

b) Propagation:

Typically, when the output variables are a complex, nonlinear function of the input variables, the PDF of which cannot be determined analytically, Monte Carlo methods are used to estimate the uncertainty. The principle of MCM is to generate the random numbers by the probability density function of input variables, their assignment in the measurement model and calculation probability function of output variables. For each iteration of the Monte Carlo process, a set of random values for the model parameters are generated.

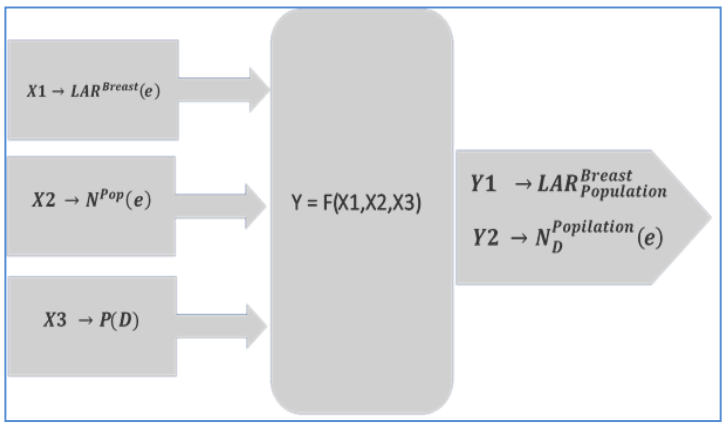

Figure 8. Illustrations of the methodologies. Propagation of uncertainties and resulting distributions

For Each input quantity X1, X2 and X3 generates M random vectors $X1_j, X2_j \; and \; X3_j$ j = 1, . . . , M according to the density of distribution of uncertainties.Thus generated $M \cdot 3$ numbers. Where the value of M was chosen from the condition $\boldsymbol{M \geq \frac{10^4}{(1-p)}}$, 100*p - represents the output variables coverage probability. We have coverage probability 90%, so p = 0,90 and M should be at least 200,000. The measurement model j-th element corresponds **X1j ,X2j, X3j** random numbers according to the uncertainty distribution density. The values **Yj, j = 1, . . . , *M*** must be sorted in the form of a histogram, the bin of which is determined by the required accuracy of the estimates. This ordered model represents a discrete distribution function **Y**, on the basis of which standard statistical indicators are calculated.

Figure 9. presents the Probability of developing radiation induced cancer as a function of age-at-exposure in a hypothetical population of women exposed to 10 mGr (rhombuses) and modeled (squares) doses. Colored area on the graphs correspond to mean ± standard deviation values.

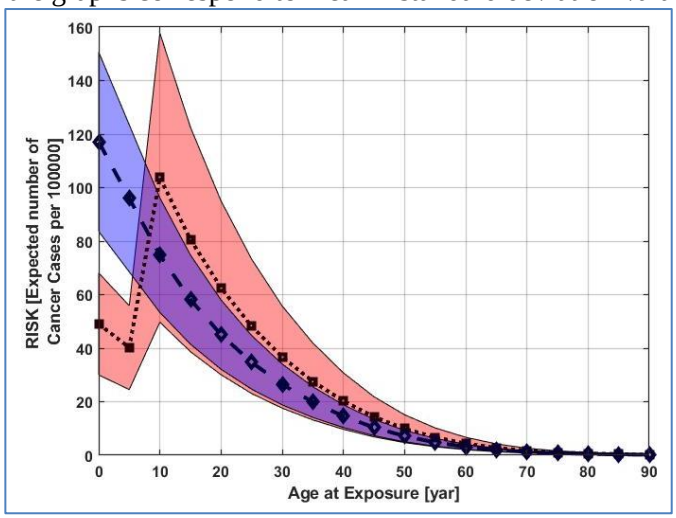

Figure 9. Probability of developing radiation induced cancer (number of additional cases per 100,000 exposed persons) as a function of age-at-exposure in a hypothetical population of women exposed to 10 mGr (rhombuses) and modeled (squares) doses. Colored area on the graphs correspond to mean ± standard deviation values

As can be seen from the graph, the colored area on the graph, corresponding to the modeled doses significantly exceeds the area corresponding to the fixed dose, which is due to the additional uncertainties associated with dose modeling.

According to our estimates, the projected number of future breast cancer cases, associated with chest CT examination of hospitalized in 2021 female COVID-19 patients is 20.06 [90% UR 5.02 - 46.96] cases, moreover, the largest number of cases is observed in the age group 10-35 at the time of exposure (Figure 10)

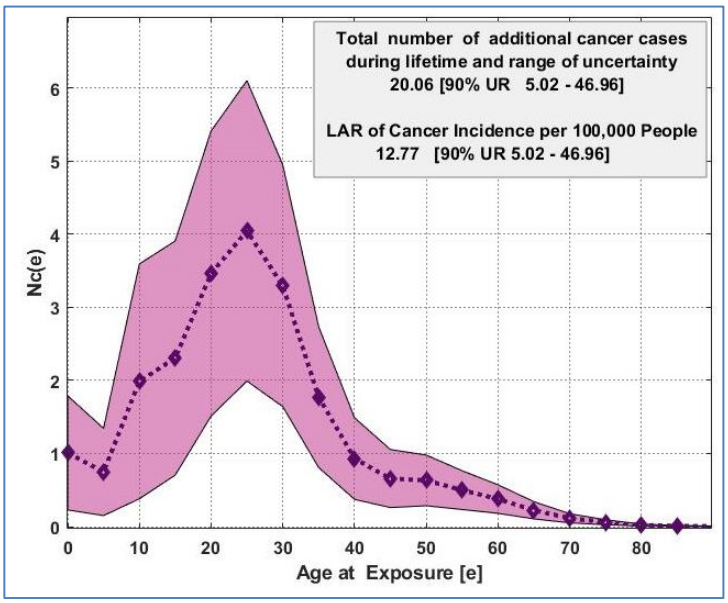

Figure 10. Prognostic values radiation-induced breast cancer cases during lifetime as a function of age at exposure, in hospitalized in 2021 female COVID-19 patients in Georgia. Colored area on the graph represents to 90% range of uncertainty.

Estimated value of the lifetime attributable risk (LAR) for Breast cancer in female COVID patients, related to chest computed tomography in one year is - 12.77 [90% UR 3.20 - 29.90] cases per 100,000 persons. In our earlier study [29], it was shown that the lifetime baseline risk of breast cancer (LBRgeo) in the Georgian female population is 6200 (UR 6500 – 6900) cases per 100,000 person, hence the risk associated with Chest CT causes a slight increase in the baseline risk for the entire population (≈0,2%), However, for the female population under 40 years of age, the ratio LAR and age-conditional baseline risk is approximately 2.2%, which is not a negligible value, considering the annual frequency of CT examinations and the cumulative effect of radiation.

DISCUSSION

The biological effects of low dose radiation and the prediction of their medical consequences have long been a subject of interest, and not only in relation to medical exposure. The intensification of research in this direction was driven by the sharp increase in the frequency of chest CT scans and, accordingly, dose loads on populations during the Covid pandemic. Studies have focused on estimating the prognostic values of CT doses and their associated carcinogenic risk in different countries and populations: In work [17] by searching various online databases: Medline, PubMed, Web of Science, Scopus, ResearchGate, medRxiv, bioRxiv and Google scholar, an extensive literature review was conducted regarding the protocols used, the dose loads and the associated carcinogenic risks in COVID-19 infected patients. Both low-dose, standard, and high-resolution protocols were discussed. It was found that the CTDIvol for standard and high-resolution protocols varied in the range of 6.8–13 mGy, DLP – in the range of 240–650 (mGy.cm), and the LAR estimated by the BEIR VII methodology varied in the range of 15–150 (cases/100,000 persons). The CTDIvol for low-dose protocols varied in the range of 1–3.5 mGy, DLP – in the range of 20–65 (mGy.cm), and the LAR estimated by the BEIR VII methodology varied in the range of 1.5–7 (cases/100,000 persons).

In the works of Italian scientists [40] The average CTDIvol, SSDE and DLP were 6.8 mGy, 8.7 mGy, 239 mGy cm respectively. The average LAR of all solid cancers was 21 cases per 100,000 patients, with breast and lung cancer localizations at the highest risk in the female population; approximately 25 cases per 100,000 patients. Relatively small risks were observed in the publication of Iranian researchers - The average LAR for all cancer types was 10.30 ± 6.03 cases per 100,000 patients. The average CTDIvol and DLP for females was 3.70 ± 6.63 mGy and 105.50 ± 48.51 mGy.cm respectively. In females, the highest equivalent doses were recorded for the lung (4.58 ± 0.60 mSv) and breast (4.06 ± 0.54 mSv).

The results obtained in our study are consistent with the literature estimates within the margin of error and for the population as a whole. the contribution of radiation exposure for 1 year is insignificant (0.2% of the LBR of breast cancer), However, for the female population under 40 accounts for 2.2% of the age-conditional probability of developing cancer.

As can be seen from the above, the increase in cancer incidence directly associated with the Covid pandemic should not be considered a cause for particular concern, but it demonstrates the need to predict the dose loads and risks associated with diagnostic radiology in the long-term (10-20 years) perspective and the relevance of assessing their share in global trends in cancer incidence in the population (permanent increase in incidence, rejuvenation of the contingent) [41-43]. The further adaptation of the BEIR VII methodology to the specifics of specific populations is a subject of separate discussion. As is known, the cancer risk estimates under BEIR VII are based on a linear no-threshold model and data collected from populations of Japan atomic bomb survivors and are thus an extrapolation. In addition, the methodology does not take into account possible interpopulation differences in radiosensitivity and for interpopulation risk transfer, a mixture of EAR and ERR risk models is used in varying proportions for different cancer sites. For breast cancer, the 100% EAR model was used, However, in recent years, strong evidence has emerged that questions the validity of using the EAR model to estimate breast cancer risk [44], in particular,

the incidence of breast cancer in the Japanese population has been steadily increasing. As a result, in the Life Span Study (LSS) of Japanese A-bomb Survivors, the ERR model currently predicts similar dose-dependent increases across age cohorts, whereas the EAR model predicts different dose-dependent increases across age cohorts. Problems with risk estimation have also been identified in a large-scale study, which, based on 111.6 million adult patients who underwent CT scans, found a plausible dose-dependent increase in cancer risk in exposed patients but highlighted the need for further development of the methodology for quantitative LAR estimates [19].

CONCLUSION

The lifetime attributable risk for Breast cancer in female COVID-19 patients in Georgia, related to chest computed tomography in one year is low - the LAR is only 0.2% of the LBR for breast cancer. However, the highest increase was seen in the 10-35 age group - for the population under 40 years old, it is 2.2% of the age-conditional probability of developing cancer. Given the cumulative effects of ionizing radiation and the potential risk of multiple or repeated scanning, further improvements in methods for predicting the long-term effects of medical radiation exposure in the population appear necessary.

REFERENCES

[1]. Davenport, M.S.; Chu, P.; Szczykutowicz, T.P.; Smith-Bindman, R. Comparison of Strategies to Conserve Iodinated Intravascular Contrast Media for Computed Tomography During a Shortage. JAMA 2022, 328, 476–478

[2]. Miglioretti, D.L.; Johnson, E.; Williams, A. Pediatric computed tomography and associated radiation exposure and estimated cancer risk. JAMA Pediatr. 2013, 167, 700–707.]

[3]. National Research Council. 2006. Health Risks from Exposure to Low Levels of Ionizing Radiation: BEIR VII Phase 2. Washington, DC: The National Academies Press.

[4]. EPA Radiogenic Cancer Risk Models and Projections for the U.S. Population, U.S. Environmental Protection Agency Office of Radiation and Indoor Air, April 2011, 1200 Pennsylvania Ave., NW Washington, DC 20460

[5]. Radiation Protection in Medicine, ICRP PUBLICATION 105, Annals of the ICRP, 2007

[6]. Amy Berrington de Gonzalez at all, RadRAT: A Radiation Risk Assessment Tool for Lifetime Cancer Risk Projection, J Radiol Prot. 2012 September ; 32(3):

[7]. Health risk assessment from the nuclear accident after the 2011 Great East Japan Earthquake and Tsunami based on a preliminary dose estimation. World Health Organization; 2013. (http://www. who.int/ionizing_radiation/pub_meet/fukushima_risk_assessment_ 2013/en)

[8]. Brenner DJ, Hall EJ. Computed tomography—an increasing source of radiation exposure. N Engl J Med. 2007; 357(22):2277–2284.]

[9]. Amy Berrington de González, Projected Cancer Risks from Computed Tomographic Scans Performed in the United States in 2007

[10]. childhood or adolescence: data linkage study of 11 million Australians, BMJ 2013;346:f2360.

[11]. Yu-Hsuan Shao at all, Exposure to Tomographic Scans and Cancer Risks. JNCI Cancer Spectrum (2020) 4(1):

[12]. Jae-Young Hong at all, Association of Exposure to Diagnostic Low-Dose Ionizing Radiation With Risk of Cancer Among Youths in South Korea, JAMA Network Open. 2019;2(9):e1910584

[13]. Mark S Pearce at all, Radiation exposure from CT scans in childhood and subsequent risk of leukaemia and brain tumours: a retrospective cohort study, Lancet 2012; 380: 499–505

[14]. Mehmet Coşkun, Did radiation exposure increase with chest computed tomography use among different ages during the COVID-19 pandemic? A multi-center study with 42028 chest computed tomography scans, Diagn Interv Radiol 2023; DOI: 10.5152/dir.2022.211043
[15]. Fatemeh Homayounieh at all, Variations in CT Utilization, Protocols, and Radiation Doses in COVID-19 Pneumonia: Results from 28 Countries in the IAEA Study, Radiology 2021; 298:E141–E151
[16]. Mannudeep K. Kalra at all, Chest CT practice and protocols for COVID-19 from radiation dose management perspective, European Radiology (2020) 30:6554–6560
[17]. Mandeep Garg at all, Radiation Exposure and Lifetime Attributable Risk of Cancer Incidence and Mortality from Low- and Standard-Dose CT Chest: Implications for COVID-19 Pneumonia Subjects, Diagnostics 2022, 12, 3043.
[18]. Jong Hyuk Lee, MD1 at all, CT Examinations for COVID-19: A Systematic Review of Protocols, Radiation Dose, and Numbers Needed to Diagnose and Predict, J Korean Soc Radiol 2021;82(6):1505-1523
[19]. Chun-Feng Cao at all, CT Scans and Cancer Risks: A Systematic Review and Dose-response Meta-analysis, BMC Cancer (2022) 22:1238
[20]. Nissren Tamam at all, Assessment of breast dose and cancer risk for young females during CT chest and abdomen examinations, Applied Radiation and Isotopes,Volume 190, December 2022, 110452
[21]. Mohammad Hossein Jamshidi at all, Estimation of Lifetime Attributable Risk (LAR) of Cancer Associated with Chest Computed Tomography Procedures in Children, Frontiers in Biomedical Technologies Vol. 10, No. 4 (Autumn 2023) 441-448
[22]. Joël Greffier at all, Ultra-low-dose chest CT performance for the detection of viral pneumonia patterns during the COVID-19 outbreak period: a monocentric experience, Quantitative Imaging in Medicine and Surgery, Vol 11, No 7 July 2021
[23]. Geoffrey D. Rubin at all, The Role of Chest Imaging in Patient Management during the COVID-19 Pandemic: A Multinational Consensus Statement from the **Fleischner Society,** Radiology: Volume 296: Number 1—July 2020.
[24]. Centers for Disease Control and Prevention. Interim Clinical Guidance for Management of Patients with Confirmed Coronavirus Disease (COVID-19). https://www.cdc.gov/ coronavirus/2019-ncov/hcp/clinical-guidance-managementpatients.html
[25]. ACR recommendations for the use of Chest Radiography and Computed Tomography (CT) for Suspected COVID-19 Infection. https://www.acr.org/Advocacy-and-Economics/ACR-PositionStatements/Recommendations-for-Chest-Radiography-and-CTfor-Suspected-COVID19-Infection].
[26]. Li Fan, ShiYuan Liu, CT and COVID-19: Chinese experience and recommendations concerning detection, staging and follow-up, European Radiology (2020) 30:5214–5216
[27]. Diagnosis and treatment protocols of COVID-19 infection (trial version 5). The National Health Commission of the People's Republic of China [EB/OL]
[28]. Mannudeep K. Kalra at all, Chest CT practice and protocols for COVID-19 from radiation dose management perspective, European Radiology (2020) 30:6554–6560
[29]. Giorgi Ormotsadze, Tamar Sanikidze, Alla Zedginidze, Levan Ormotsadze, radiogenic breast cancer risk projection for the Georgian female population, Journal of Radiobiology and Radiation Safety Vol.4, №5, 2024
[30]. International standard iso 31000, Risk management **— Guidelines**, Second edition 2018-02;

[31]. Joint Committee for Guides in Metrology (JCGM), Guide to the Expression of Uncertainty in Measurement (GUM) 100-208, "Evaluation of measurement data — Guide to the expression of uncertainty in measurement"],

[32]. Joint Committee for Guides in Metrology (JCGM), "Evaluation of measurement data — Supplement 1 to the "Guide to the expression of uncertainty in measurement" —Propagation of distributions using a Monte Carlo method",

[33]. IPCS risk assessment terminology. Part 1: IPCS/OECD key generic terms used in chemical hazard/risk assessment. Part 2: IPCS glossary of key exposure assessment terminology. Geneva, World Health Organization, International Programme on Chemical Safety (Harmonization Project Document No.)

[34]. Kemeny, J. et al., Report of the President's Commission on the Accident at Three Mile Island, Washington, DC, 1979;

[35]. Health and Safety Executive, Safety Assessment Principles for Nuclear Plants, HMSO, London, 1992

[36]. Guidance for Industry and FDA Staff , Guidance for the Use of Bayesian Statistics in Medical Device Clinical Trials. Food and Drug Administration 5630 Fishers Lane, Rm 1061, Rockville, MD 20852, 201;

[37]. Benefit-Risk Assessment for New Drug and Biological Products Guidance for Industry, U.S. Department of Health and Human Services Food and Drug Administration Center for Biologics Evaluation and Research (CBER) Center for Drug Evaluation and Research (CDER) October 2023.

[38]. [Schaller T, Hirschbühl K, Burkhardt K, et al. Postmortem examination of patients with COVID-19. JAMA 2020;323(24):2518–2520

[39]. Daniela Ghio at all, Demographics of COVID-19 hospitalisations and related fatality risk patterns, Health policy 126 (2022) 945–955]

[40]. C. Ghetti at all, Dosimetric and radiation cancer risk evaluation of high-resolution thorax CT during COVID-19 outbreak, Physica Medica 80 (2020) 119–124

[41]. Jon Shelton at all, 25 year trends in cancer incidence and mortality among adults aged 35-69 years in the UK, 1993-2018: retrospective secondary analysis, BMJ 2024;384:e076962 | doi: 10.1136/bmj-2023-076962;

[42]. Xiao-Wei Tang at all, Long-term trends in cancer incidence and mortality among U.S. children and adolescents: a SEER database analysis from 1975, Front Pediatr. 2024 Jul 5:12:1357093;

[43]. Yan Zhou at all, Long-term trends of lung cancer incidence and survival in southeastern China, 2011– 2020: a population-based study, BMC Pulmonary Medicine (2024) 24:25

[44]. L. Walsh et al, A Framework for Estimating Radiation-Related Cancer Risks in Japan from the 2011 Fukushima Nuclear Accident, Radiation research 182, 556–572 (2014)

[45]. Mossa-Basha M, Meltzer CC, Kim DC et al (2020) Radiology department preparedness for COVID-19: radiology scientific expert panel. Radiology. 16:200988